A&A 418, 727–736 (2004)
DOI: 10.1051/0004-6361:20035638

Astronomy & Astrophysics

Photospheric and stellar wind variability in ϵ Ori (B0 Ia)⋆

R. K. Prinja[1], Th. Rivinius[2], O. Stahl[2], A. Kaufer[3], B. H. Foing[4], J. Cami[5], and S. Orlando[6]

[1] Department of Physics & Astronomy, University College London, Gower Street, London WC1E 6BT, UK
[2] Landessternwarte Heidelberg, Königstuhl 12, 69117 Heidelberg, Germany
[3] European Southern Observatory, Alonso de Cordova 3107, Casilla 19001, Santiago 19, Chile
[4] Research Support Division, ESA RSSD, ESTEC/SCI-SR postbus 299, 2200 AG Noordwijk, The Netherlands
[5] NASA Ames Research Center, Mail Stop 245-6, Moffett Field, CA 94035-1000, USA
[6] INAF-Osservatorio Astronomico di Palermo, Piazza del Parlamento 1, Palermo, Italy

Received 6 November 2003 / Accepted 17 January 2004

Abstract. We provide direct observational evidence for a link between photospheric activity and perturbations in the dense inner-most stellar wind regions of the B supergiant star ϵ Ori. The results, which are relevant to our understanding of the origin of wind structure, are based on a multi-spectral line analysis of optical time-series data secured in 1998 using the HEROS spectrograph on the ESO Dutch 0.9-m telescope in La Silla. A period of ∼1.9 days is consistently identified in Balmer, He I absorption, and weak metal lines such as Si III and C II. The primary characteristic is a large-amplitude swaying of the central absorption trough of the line, with differential velocities in lines formed at varying depths in the atmosphere. The variance resulting from the "S-wave" velocity behaviour of the lines is constrained within ± the projected rotation velocity (∼80 km s^{-1}) in the weakest absorption lines, but extends blue-ward to over −200 km s^{-1} in Hα. A second (superimposed) 1.9 day signal is present at more extended blue-ward velocities (to ∼−300 km s^{-1}) in lines containing stronger circumstellar components. Inspection of archival optical data from 1996 provides evidence that this modulation signal has persisted for at least 2.5 years. Non-radial pulsational modelling is carried out in an attempt to reproduce the key observational characteristics of the line profile variability. Only limited success is obtained with prograde ($m = -1$) modes. The principal S-wave pattern cannot be matched by these models and remains enigmatic.

Key words. stars: early-type – stars: individual: ϵ Ori – stars: mass-loss – stars: oscillations

1. Introduction

One of the important unresolved issues in massive star astrophysics is whether fluctuations at the stellar surface can act as the primary trigger for the formation of organised large-scale structure in their line-driven winds. The observational and theoretical hunt for this "connection" is motivated by the fact that, (i) wind variability in OB stars (e.g. as evident in UV resonance lines) is often modulated or quasi-cyclic, on variability time-scales that may relate to stellar rotation periods (e.g. Massa et al. 1995; de Jong et al. 2001; Prinja et al. 2002), and (ii) high-quality optical spectroscopic data sets have revealed subtle line profile variability in O and early B-type stars, that may be interpreted as the action of surface velocity fields due to non-radial pulsations (e.g. Fullerton et al. 1996, and reviews by Baade 1997; Henrichs 1998).

However, the pattern of stellar wind variability is not always coherent or even obviously repetitive, and furthermore the pulsation characteristics may be complicated by multi-periodicity and latitude dependence. Consequently any potential connection between stellar wind and photospheric activity may not be a simple ("linear") one, and could be more enigmatic due to the co-addition of signals and time-scales. There have nevertheless been some observational successes regarding the wind-photosphere connection in luminous early-type stars. For example, Reid & Howarth (1996) detected a low-degree pulsational mode in ζ Pup (O4 Inf) with a period of 8.5 h. While other modes may also be present, the 8.5 h period was also detected in the blue wing of the Hα emission. In the O7.5 III star ξ Per, de Jong et al. (2001) traced a ∼2 day (UV) wind modulation down to near-photospheric velocities, though they only detected pulsational periods on much shorter time-scales (∼3.5 h). Time-series analysis of line profile variability across the Hα profile of HD 64760 (B0.5 Ib) by Kaufer et al. (2002) revealed a 2.4 day pattern in the velocity widths (i.e. at ± projected rotation velocity), which is in excellent agreement with the outer wind periods previous established

Send offprint requests to: R. K. Prinja,
e-mail: rkp@star.ucl.ac.uk

⋆ Based on observations obtained as part of the MUSICOS 98 campaign from ESO La Silla, Chile.

Table 1. Fundamental parameters for ϵ Ori.

Parameter	Value	Reference
Spectral Type	B0 Ia	Walborn (1976)
$T_{\rm eff}$	28 500	Kudritzki et al. (1999)
$v_{\rm e}\ \sin(i)$	80 km s^{-1}	Kudritzki et al. (1999)
$R_\star/R_\odot$	35	Kudritzki et al. (1999)
$M_\star/M_\odot$	20	Schaller et al. (1992)
V_∞	1500 km s^{-1}	Kudritzki et al. (1999)
$\dot{M}$	$1.9 \times 10^{-6}\ M_\odot$ yr^{-1}	Blomme et al. (2002)
$P_{\rm rot}$(max)	~22 days	

using *IUE* ultraviolet spectroscopy. As a wider example, the connection between pulsation and mass-loss has been observed in the B (emission) star μ Cen (Rivinius et al. 1998), where the constructive interference of several non-radial pulsation modes is strongly correlated with circumstellar outbursts.

In this paper we present high quality optical ("blue" and "red") time-series spectroscopy of the early B-type supergiant ϵ Ori (HD 37128, B0 Ia, middle star in the Belt of Orion). The principal aim of this work is to compare the variability characteristics of wind and wind/photosphere transition lines (Hα emission and Balmer absorption) to photospheric fluctuations in weaker absorption lines due to He I and metals such as Si III λ4553 and C II λ4267. Previously, variability on the time-scale of days has been noted in the Hα profile of ϵ Ori (e.g. Ebbets 1982; Levato et al. 1988; Scuderi 1994). Though absorption line radial velocity shifts have also been detected (e.g. Morrell & Levato 1991), ϵ Ori is not known to be a spectroscopic binary (e.g. Jarad et al. 1989). It is the only "normal" early-B supergiant with a measured thermal radio flux, and Blomme et al. (2002) discount previous suggestions that it is a *variable* thermal radio source. Some fundamental parameters of the star are given in Table 1, none of which are particularly exceptional for a star of this spectral type and luminosity class. The ultraviolet resonance lines of ϵ Ori are variable on hourly time-scales, due to the blue-ward progression of discrete absorption components (DACs, e.g. Prinja et al. 2002). The *IUE* data sets are not extensive enough to establish (or rule out) a repetitive or cyclic behaviour. In the X-ray band, Cassinelli et al. (1983) and Collura et al. (1989) did not find any variability in the Einstein Observatory (IPC) data of ϵ Ori.

We present here photospheric and stellar wind variability results primarily from a time-series optical monitoring campaign carried out during November and December 1998. The investigation focuses on evidence that stellar surface perturbations propagate into the inner wind regions of the early-B supergiant star.

2. Observations and data reduction

This paper is primarily based on a 17-night spectroscopic observing run carried out between November 26, 1998 and December 13, 1998 using the ESO Dutch 0.9-m telescope at La Silla with the HEROS spectrograph. Originally these data were part of the 1998/1999 *Musicos* multi-site campaign (e.g. Foing et al. 1999). The only other comparable time-series of ϵ Ori from this project were secured over 8 nights from the Observatoire Haute Provence (OHP), France from Aurelie at the 1.52-m telescope. However these data suffered from severe problems of structure in flat-field frames, and we are forced to conclude that they are not suitable for a study of subtle line profile variability.

The HEROS spectra are divided into two channels after the echelle grating. Each channel has its own cross-disperser, camera and detector. The blue one covers the wavelength range $\lambda\lambda$3450 Å to 5560 Å and the red one covers $\lambda\lambda$5820 Å to 8620 Å. The spectral resolution ($\lambda/\Delta\lambda$) is ~20 000 in both cases. Pipe-line data reduction was carried out using a modified version of the ESO-Midas echelle context (e.g. Stahl et al. 1995). Typically the signal-to-noise of the individual spectra is ~200, and the (internal) stability of the velocity scale in the extracted spectra is ~2 km s^{-1}. The final HEROS data set from 1998 of ϵ Ori comprises of 61 spectra per channel over ~17.3 days, with a typical sampling of 4 spectra per night (i.e. ~8 h). Throughout this paper we have corrected (to the stellar rest frame) for a radial velocity of 26 km s^{-1}.

In order to study the longer-term behaviour of the optical lines, we also present here some archival data of ϵ Ori which were secured over several months in 1996 as part of the Heidelberg extended monitoring campaign of massive stars.

3. Line profile variability

ϵ Ori is a good candidate for studying the origin of stellar wind structure since it has active UV and optical wind lines and the star is not obviously peculiar in terms of luminosity, wind density, stellar rotation, binary interaction and so on. The mean "blue" spectrum from the HEROS time-series is shown in Fig. 1; the dominant absorption due to Balmer and He I lines is as expected for a B0 Ia star. (Overall, the optical spectrum is very similar to that of e.g. HD 204172; B0 Ia and κ Ori; B0.5 Ia). The lower panel in Fig. 1 gives an indication of the maximum variability present in Hα. The total equivalent width of the line can change by a factor of 4 (the mean total (absorption "plus" emission) value in our data set is ~0.2 Å). The strong underlying photospheric absorption and the wind emission components are both potential contributors to these fluctuations and we comment further on these below. The absorption equivalent width of Hβ and Si III λ4553 vary by factors of up to ~30% and 15%, respectively.

The principal form of the absorption line profile variability in ϵ Ori is striking and a clear illustration of it is presented in Fig. 2, using a typical pair of HEROS spectra separated by ~1 day. There are several important points to note: The absorption line profiles "sway" in central velocity by substantial amounts, but the *amplitude of this motion is not the same for different lines.* There is also evidence for variable structure ("humps") in the blue and red wings of the broader Hβ and Hγ absorption troughs. The peak-to-peak shift in the velocity at which absorption minimum occurs (for example) is greatest in Hβ (~±60 km s^{-1}) and Hγ (~±40 km s^{-1}), intermediate for He I λ5876 (~±30 km s^{-1}) and He I λ6678 (~±30 km s^{-1}), and lowest for Si III λ4553 (~±20 km s^{-1}) and He I λ4713 (~±15 km s^{-1}). (Incidentally, the interstellar Na I lines at ~λ5890 serve as excellent wavelength fiducials

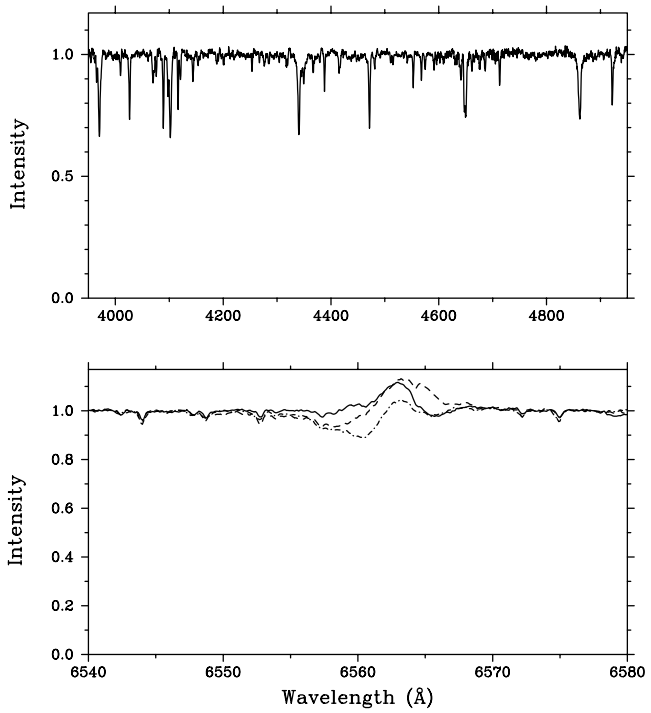

Fig. 1. Mean of the 61 "blue" HEROS optical spectra of ϵ Ori from 1998 (*upper panel*). Examples of the maximum changes present in the Hα profile are shown in the lower panel.

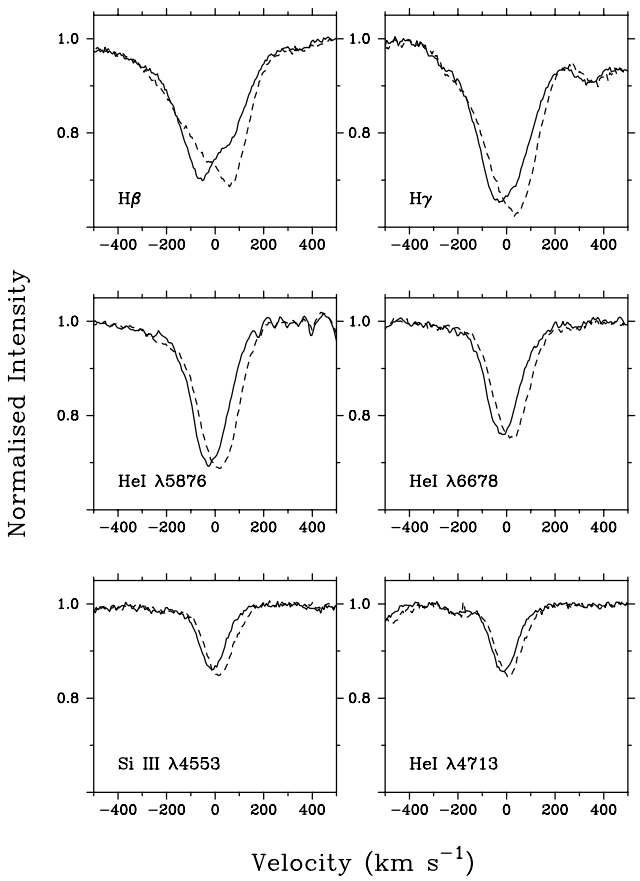

Fig. 2. Differential behaviour in the velocity amplitudes of the line profile changes in Balmer, He I and metal lines is evident in two spectra separated by ~24 h.

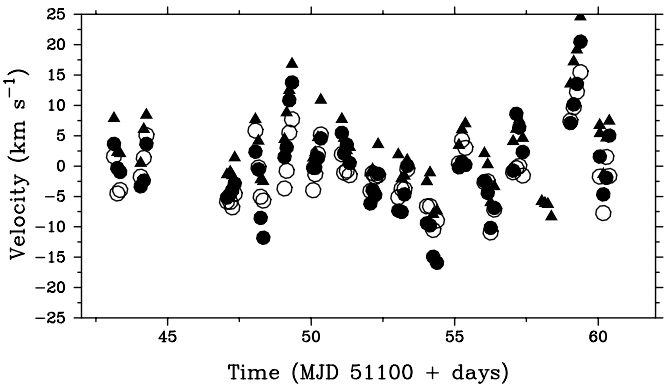

Fig. 3. Central absorption velocities as a function of time for Hγ (filled circles), He I λ6678 (filled triangles) and Si III λ4553 (open circles).

for the He I λ5876 velocity shifts.) As an alternative to recording the mode of the absorption troughs, Gaussian profile fitting was used to compare the central velocities of Hγ, He I λ6678, and Si III λ4553. (In these three cases the absorption profiles are generally symmetric and well matched by a Gaussian model.) The results of the fits are shown in Fig. 3. The maximum velocity displacements are greater for Hγ and He I λ6678 (i.e. $\sim\pm$20 km s^{-1}) than Si III λ4553 ($\sim\pm$10 km s^{-1}). For an individual spectral line there is no systematic difference in the absorption strength between blue-ward and red-wards shifted features. The lines discussed above are of course formed at different depths in the atmosphere of ϵ Ori. The differences in the velocity displacements measured between them may in part be due to a velocity gradient through the atmosphere. Note, however, that the individual lines do not exhibit blue-ward asymmetries, and the overall trend in velocity as a function of time is well matched between the 3 spectral lines, with no measurable evidence for lags.

The line profile changes in ϵ Ori are compared in Fig. 4 between Balmer, He I and weak metal lines using grey-scale image representations (dynamic spectra) of variability over ~17 days. To enhance the contrast of the profile changes, quotient spectra are displayed after being normalised by the mean profile of the full time-series. (Lighter shades indicate regions of reduced absorption or enhanced flux, with respect to the mean profile.) The presence of activity blue-ward and red-ward of line centre is expected, given the swaying profiles already highlighted in Fig. 2. It is important to note that the basic variability pattern is the same for all the lines in Fig. 4. In particular, though Hα has a strong wind emission component, the profile changes are mimicked not only in other Balmer and relatively strong He I lines, but also in much weaker and narrower lines such as He I λ4713 and Si III λ4553. The impression therefore is that the same underlying absorption changes that affect the weak He I and metal lines, also act in a sympathetic manner in Hα. However, the variability in Hα extends beyond the projected rotation velocity of ϵ Ori (~80 km s^{-1}, Table 1). We do not find any evidence in these data for systematic time-lags in the activity between different lines. The cross-correlation of the quotient spectra of Hβ and Si III λ4553 results in a shift in the

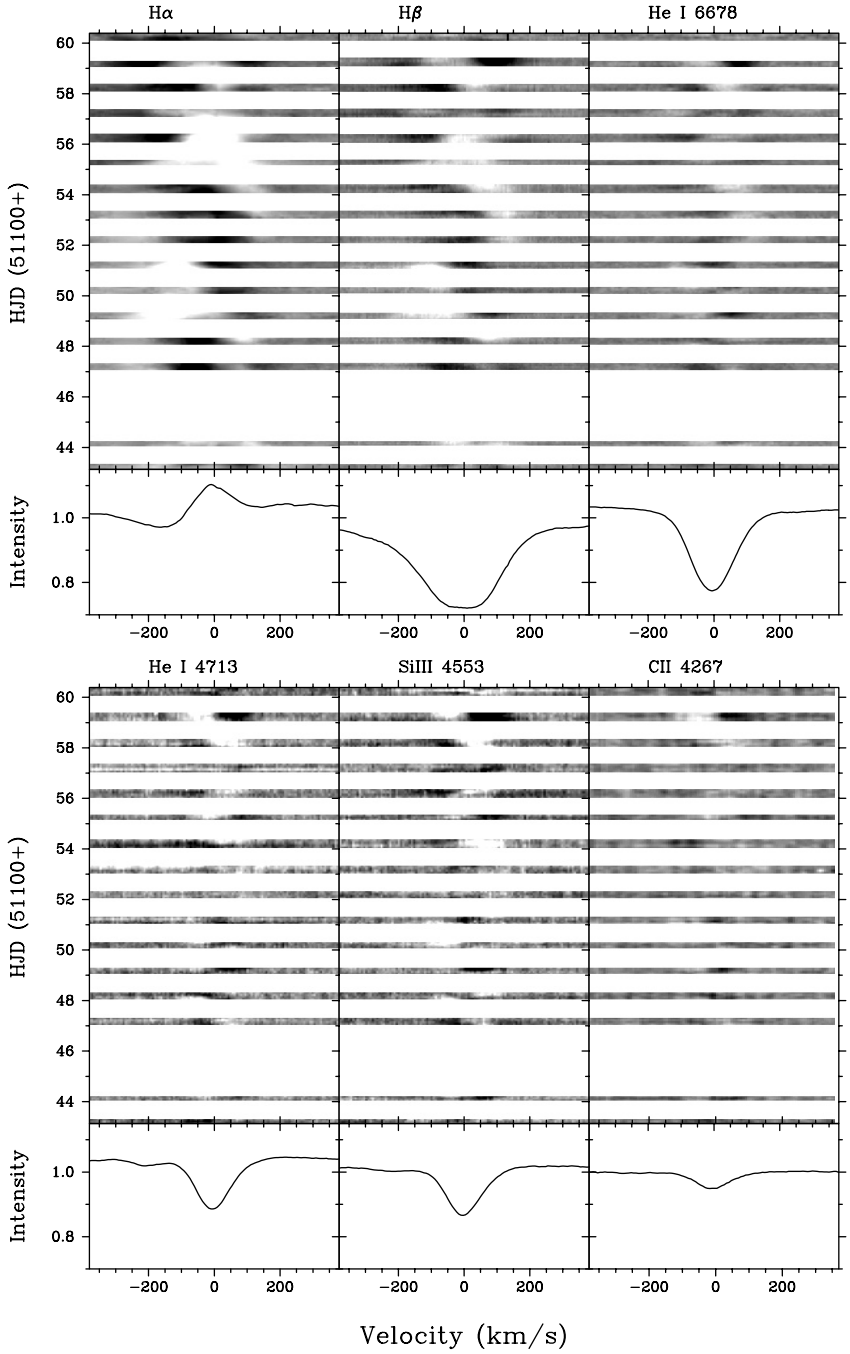

Fig. 4. Grey-scale representations of the line profile variability in ϵ Ori. Darker shades indicate enhanced absorption (reduced flux) with respect to the mean profile, which is shown below each image. The scales for the three images in the upper panels correspond to differences from the mean of +5% (white) and −5% (black). For He I, Si III and C II in the lower panels the scales are +2% (white) and −2% (black). Note the similarity in the patterns evident at low velocities between the different spectral lines shown here, including between the Balmer and weak metal lines.

variability patterns of barely 10 km s^{-1}, which we do not regard as significant as the cross-correlation peak is too broad.

The important result to note here is that it not necessarily correct to invoke wind emission variability as being the sole cause of the fluctuations seen in the Hα line profiles (e.g. Fig. 1, lower panel). The good correspondence between structures seen at low velocities in the grey-scale images (Fig. 4; see also Fig. 2) raises the likelihood of variability in the underlying absorption components contributing substantially to the Hα behaviour in ϵ Ori.

3.1. Time-series analyses

We carried out a periodogram analysis to search for evidence of repetitive or cyclic properties in the line profile changes of ϵ Ori. The basic Fourier method involved uses the iterative

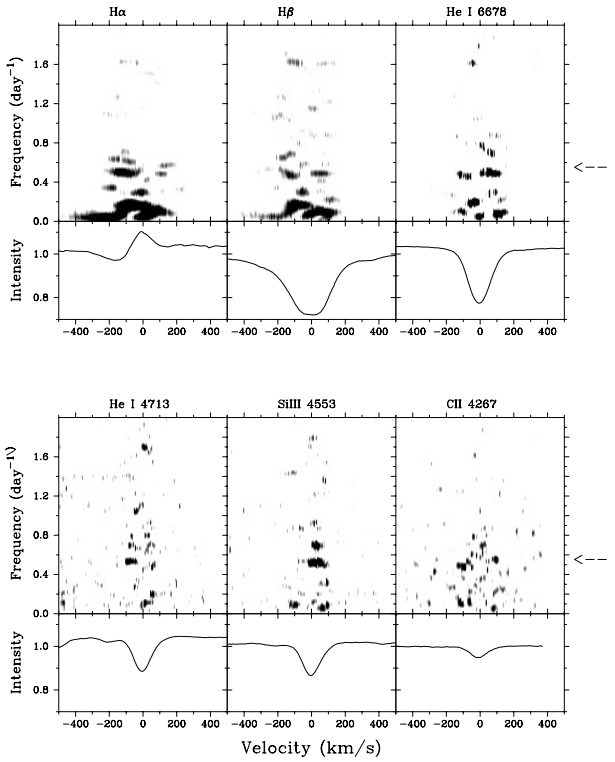

Fig. 5. Results from a Fourier analysis of the line profile variability. The power signal at frequency ~0.52 d^{-1} (arrowed) is the most consistent one in several spectral lines formed at different depths in the atmosphere of ϵ Ori

CLEAN algorithm (Roberts et al. 1987) to deconvolve the features of the window function from the discrete Fourier transform. Two-dimensional grey-scale representations of the periodograms are shown in Fig. 5 for Balmer, He I and metal lines. (A gain of 0.5 with 100 iterations was used.) Dark horizontal bands in Fig. 5 represent regions across a line profile where power is consistently present.

The primary frequencies identified are listed in Table 2. The most consistently present signal is at a frequency of ~0.52 d^{-1} (i.e. period ~1.9 days). Power at this frequency is spread significantly blue-wards in Hα, and to a lesser degree in Hβ and He I λ6678. It is more symmetric around rest velocity in He I λ4713 and Si III λ4553. There is evidence for multi-periodic behaviour in the optical absorption lines: a modulation time-scale of ~6.5 days (frequency ~0.15 d^{-1}) is present in Hα, Hβ and less prominently in He I λ6678. This signal is not detected in lines that are less affected by circumstellar contributions. An even longer time-scale of ~9.5 days is tentatively identified in the Balmer lines, but remains highly uncertain, partly as it is blended with low frequency power corresponding to the total length of the observing run. The sampling of our HEROS data of 4 to 5 spectra per night is not intensive enough for a reliable study of power at much shorter periods (i.e. few hours) than discussed above.

The ~1.9 day period is the most prominent one in our optical data of ϵ Ori, and the results in Fig. 5 suggest that it is present in weak photospheric lines as well as stronger lines which additionally diagnose the inner stellar wind regions. The

Table 2. Periodic frequencies in the optical data of ϵ Ori.

Spectral line	f_1 (d^{-1})	f_2 (d^{-1})	f_3 (d^{-1})	Range of variance (km s^{-1})
Hα	0.52 ± 0.03	0.15 ± 0.03	0.09 ± 0.05	−460 to +275
Hβ	0.49 ± 0.04	0.15 ± 0.03	0.12 ± 0.06	−290 to +260
He I λ6678	0.50 ± 0.04	0.16 ± 0.07	0.10 ± 0.04	−230 to +220
He I λ4713	0.53 ± 0.07			−90 to +150
Si III λ4553	0.53 ± 0.05			−90 to +170
C II λ4267	0.52 ± 0.07			−90 to +90
Mean period (days)	~1.9	~6.6	~9.7	

Conservative errors are assigned based on the half-width at half-maximum of the power spectra profiles.

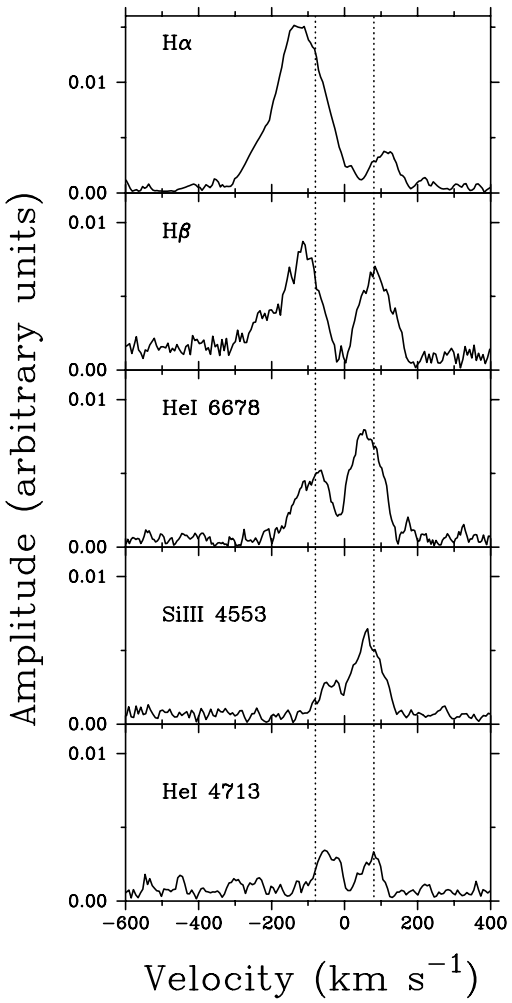

Fig. 6. The semi-amplitude of periodic signal at $P \sim 1.9$ days is shown for several lines as a function of velocity. The dotted vertical lines mark $\pm v_e \sin(i)$, the projected rotation velocity. Note the greatly increased amplitude in the blue wing of the Balmer lines, extending beyond $v_e \sin(i)$, compared to the weaker metal absorption lines.

semi-amplitude as a function of velocity at the 1.9 day period is shown in Fig. 6 for several spectral lines. The dotted vertical lines in the figure mark $\pm v_e \sin(i)$ (the projected rotation velocity). In the cases of the weak He I λ4713 and the

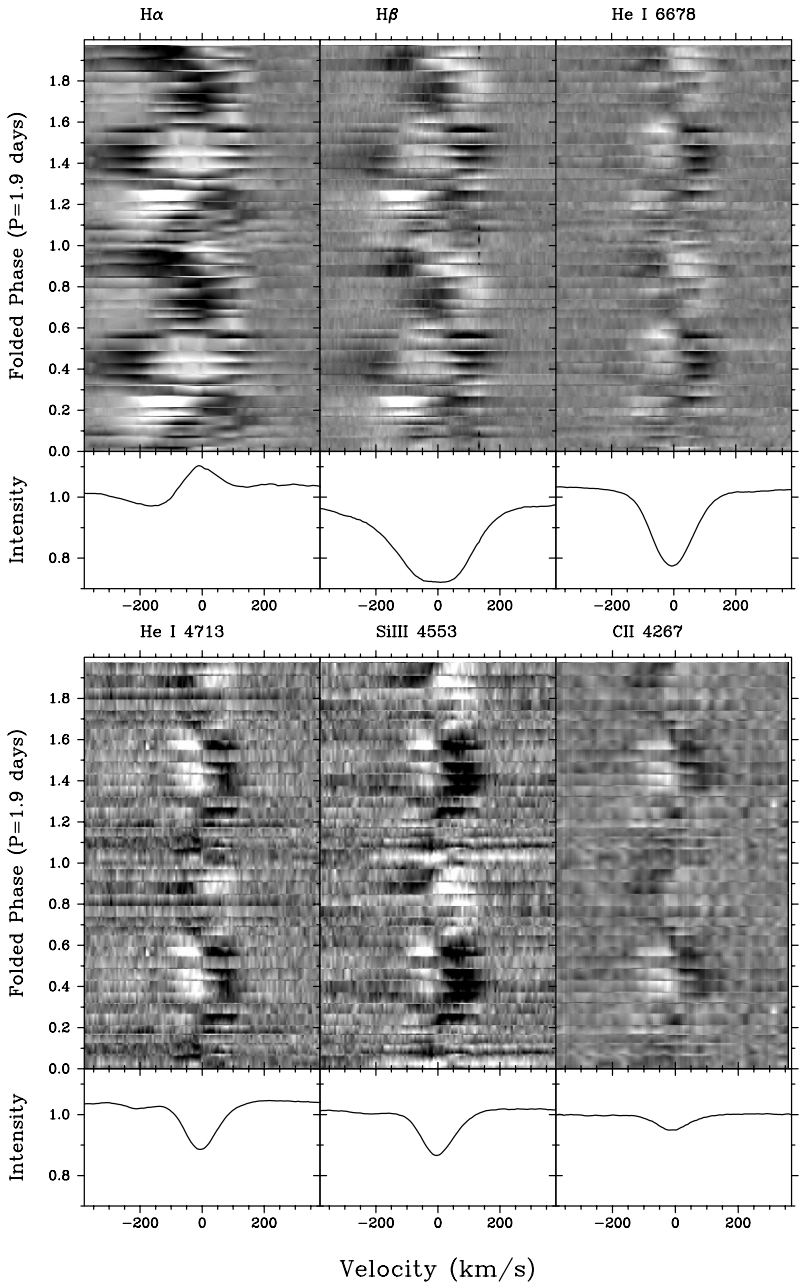

Fig. 7. Grey-scale representations of the modulated line profile changes in ϵ Ori. Individual quotient spectra (with respect to the mean) are shown plotted as function of the 1.9 day period, folded over 2 cycles. A distinctive "S-wave" modulation is clear in the weak lines. It is also present in Hα and Hβ, but in these cases an additional outer wave is super-imposed that is asymmetric to the blue and half-a-cycle out of phase with the lower velocity pattern.

Si III λ4553 line the variability due to the 1.9 day periodic component is primarily within v_e sin(i). However it clearly extends blue-wards in the Balmer lines, with an increasing amplitude. In Hα the amplitude at 1.9 days is evident out to $\sim$0.2 v_∞. The double-peaked structure of the semi-amplitude mostly reflects the blue-ward and red-ward motion of the central absorption velocity in these lines (e.g. Fig. 2). We conclude that the 1.9 day modulation discovered here provides evidence that the supersonic deep-seated wind region of ϵ Ori is responding *directly* to the photospheric activity. We acknowledge that the photospheric component of the Balmer lines in ϵ Ori are expected to have wings that extend beyond $v_e \sin(i)$ due to the effects of pressure broadening. However, the characteristics of the variability behaviour do not support pressure broadening as being responsible for the extended variability pattern in the Balmer lines since (i) we would then expect to see shifts of the entire line wings, which is not the case, (ii) the outer wings do not vary significantly, and (iii) there is still substantial power between ~ -100 to -300 km s^{-1}.

The phase-folded behaviour of the lines is complex and appears to include effects due to the superposition of different patterns. Grey-scale representations of the individual quotient (with respect to the mean) line profiles, phased on the 1.9 day

period are shown in Fig. 7, folded over 2 cycles. (Phase zero is arbitrarily set to the first spectrogram in the time-series.) The He I 4713, Si III 4553 and C II 4267 absorption lines reveal an almost identical *"S-wave" pattern*, where the initial blue-to-red excursion (from approximately $-v_e \sin(i)$ to $+v_e \sin(i)$) over the first half of the cycle is followed by a 'corresponding' red-to-blue motion. This S-wave motion contrasts with the usual repeating blue-to-red ("barber pole") patterns seen in OB stars, due to velocity fields arising from non-radial pulsations. We discuss the role of pulsations, including the specific case of near-pole on views, in more detail in Sect. 4.

The same basic "S-wave" pattern is also seen (Fig. 7) in Hα, Hβ and He I λ6678, but with higher velocity amplitudes (e.g. extending red-wards to $\sim$180 km s^{-1} in the Balmer lines and in He I λ6678). The phase of the wave is essentially the same for the 6 different spectral lines shown in Fig. 7. What is additionally striking however is that the major blue-ward variation in the Balmer lines (out to ~ -350 km s^{-1} in Hα) is due to an *additional superimposed pattern* that is (i) asymmetric to the blue, and (ii) half a cycle out of phase from the lower velocity wave, which dominates in He I λ4713, Si III λ4553 and C II λ4267 (and is symmetric about rest velocity). The (blue-ward shifted) outer-wave is stronger in Hα than in Hβ, and is weakest in He I λ6678. The outer wave is therefore more dominant in lines expected to include a greater circumstellar contribution. The physical origin and relation between the superimposed waves is obviously a key to understanding the wind-photosphere connection in ϵ Ori.

3.2. Long-term behaviour

We have thus far presented results from the intensive time-series secured between November and December 1998. In order to examine the longer-term behaviour, data collected between January and May 1996 was also examined, when ϵ Ori was included as one of the targets in the long-term monitoring program carried out by the team at Landessternwarte, Heidelberg (e.g. Stahl et al. 1996). These data were also secured using the HEROS spectrograph, but this time mounted on the ESO 50-cm telescope at La Silla, Chile. The observing strategy of these campaigns was to secure $\sim$1 spectra per night over several weeks and months for a sample of massive stars. In the case of ϵ Ori we examined 103 spectra taken over 99 days in 1996.

The mean line profiles of the time-series in 1996 and 1998 are in good overall agreement, with comparable absorption equivalent widths in Hβ and He I lines. There is no indication therefore of any gross changes in the star between these epochs, in terms of e.g. wind density or luminosity. The poorer signal-to-noise of the 1996 data makes them generally less suitable for a study of subtle line profile changes. Furthermore, the 1 per day sampling of the 1996 time-series hinders the detection of periods close to (or at multiples of) this value. Nevertheless, we show in Fig. 8 the quotient (with respect to the mean profile) individual spectra for Hβ, He I λ 4922 and He I λ4713, all phased on the 1.9 day period derived in Sect. 3.1. In all 3 cases there is evidence in the 1996 data for a "S-wave", which is very reminiscent of the patterns seen in 1998 (cf. Fig. 7). The velocity amplitudes are also broadly in agreement. The absolute phasing in Fig. 8 is arbitrary, and we cannot claim in these data that it is consistent over the numerous cycles between 1996 and 1998. What is clear is that $\sim$1.9 day period is ϵ Ori is present in the earlier seasons. The longer modulation time-scales identified in Sect. 3.1 of $\sim$5.2 days (and tentatively 9.8 days) are not confirmed in the more extended 1996 time-series.

Unfortunately there is no suitable data set in the *IUE* archive to test for a $\sim$1.9 day modulation in the stellar wind-formed UV resonance lines of ϵ Ori. Prinja et al. (2002) highlighted variability between ~ -900 to -1200 km s^{-1} in Si III λ1207, Si IV $\lambda\lambda$1400, and N V $\lambda\lambda$1240, due to the progression of a "discrete absorption component" (DAC). We have additionally inspected a set of 10 high-resolution *IUE* spectra of ϵ Ori taken over $\sim$10 days in 1987. As expected, this sparse data set does not provide any unambiguous evidence for a variability pattern on $\sim$1.9 days. One DAC-like episode is evident in Si IV $\lambda\lambda$1400, together with a gradual (over $\sim$days) decrease in the absorption strength between the blue-ward limit of the black (saturated) absorption trough in C IV $\lambda\lambda$1550 and the velocity at which the blue-ward wing intersects the local continuum ($v_{\rm edge}$).

4. Non-radial pulsation modelling

4.1. Modelling technique and parameters

In order to test whether the 1.9 day S-wave pattern might be explained by non-radial pulsation (*nrp*), we computed models for a number of parameter sets with the code by Townsend (1997). Details of the code implementation used can be found in Maintz et al. (2003, and references therein).

The stellar parameters given in Table 1 were used as base line values, i.e. $T_{\rm eff} = 28\,500$ K, $R_\star = 35\,R_\odot$, $M_\star = 20\,M_\odot$. For each set of pulsational parameters (see below) five models were computed for the rotational velocities $v = 100, 140, 180, 220,$ and 260 km s^{-1}. The inclination i was derived by requiring $v \sin i = 80$ km s^{-1}. The range for pulsational mode parameters, ℓ and m, to be probed can be constrained from the observed period, the properties of the *lpv*, and the stellar parameters: the characteristics of the *lpv* limits the potential ranges of ℓ and m to rather low values less than about three, as otherwise more than one absorption bump would be visible at any time (see e.g. Telting & Schrijvers 1997). The sign of m, i.e. whether the pulsation would have to be prograde or retrograde, can also be constrained.

The bumps propagate from the blue to the red side of the profile, i.e. for the observer the variations travel apparently prograde. A pulsational wave could still be retrograde in the co-rotating frame, though, if the star would rotate more rapidly than the wave travelling against the sense of rotation. However, the rotational period of ϵ Ori must be between 8 and 22 days, constrained by critical rotation and equatorial orientation (so that $v \sin i = v_{\rm rot}$), respectively. If the wave pattern was retrograde in the co-rotating frame, the super-period, i.e. $mP_{\rm obs}$, would have to be longer than the rotational period. Since the observed *lpv* period is only 1.9 day, values of m of at least 4

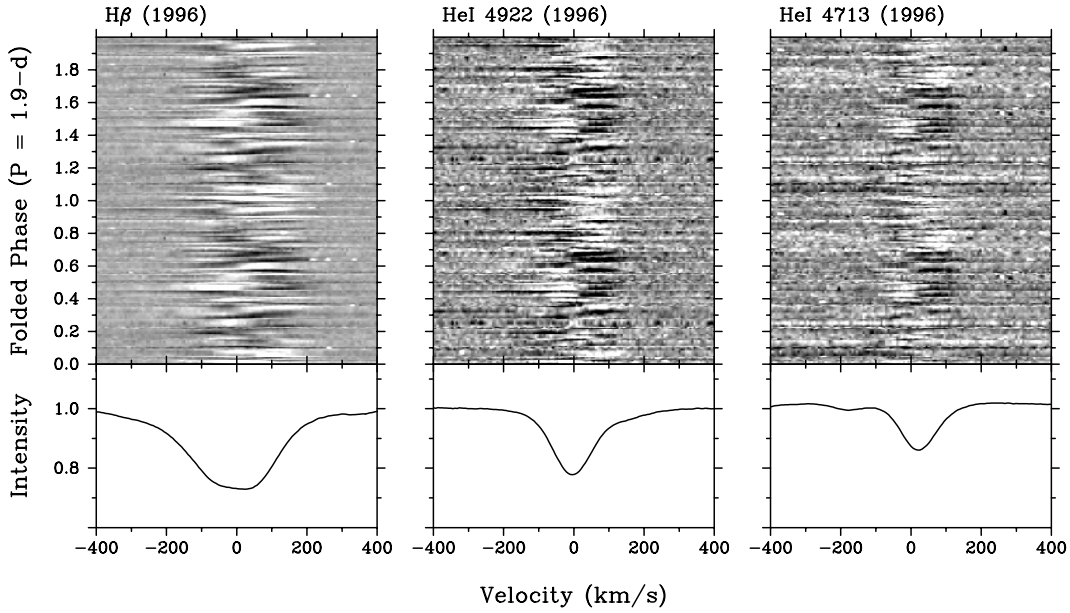

Fig. 8. The Hβ, He I λ4922 and He I λ4713 quotient spectra from the earlier (1996) season are plotted on the 1.9 day period identified in Sect. 3.1 (for the 1998 data set). This signal clearly persists over at least 2.5 years.

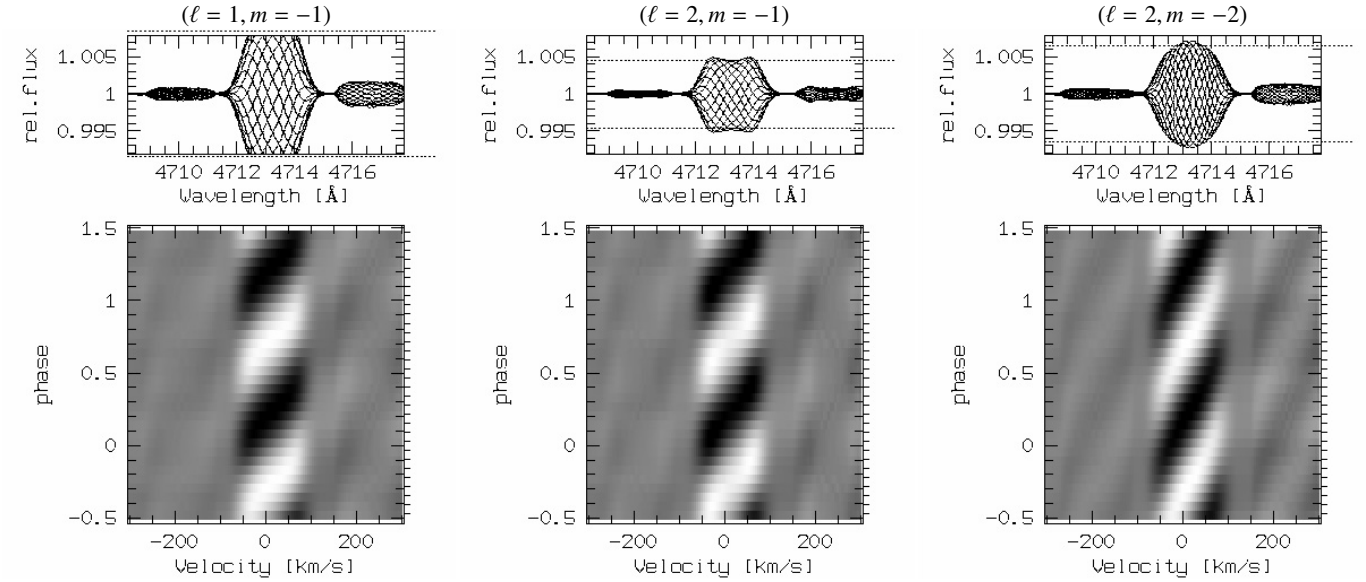

Fig. 9. Non-radial pulsation models for the three models computed for He I λ4713. Residuals against the mean computed profile are shown for the models for $v = 100\,\mathrm{km\,s^{-1}}$.

or 5 would be required even for a critically rotating star, which is not reconcilable with the actual appearance of the *lpv*.

The modes for which we opted to compute models are ($\ell = 1, m = -1$), ($\ell = 2, m = -1$), and ($\ell = 2, m = -2$). A pulsational amplitude of only 1 $\mathrm{km\,s^{-1}}$ was enough to produce variations of the order of 0.5% of the continuum, which is about the same amplitude as observed in the line chosen for modelling, namely He I 4713.

The stellar parameters result in a quite low $\log g$, at the very border of the parameter range for which synthetic spectra are implemented to the model. According to cross checks, performed with models with higher stellar mass, the absolute line profiles should not be used for comparison to the data. However, the residual variability turned out to be more robust against these limitations, and therefore only they are considered here in assessing whether non-radial pulsation is able to reproduce the observed variations.

4.2. Modelling results

None of the computed models reproduce the observed line profile variability completely. Some, however, do so better than others, and it might be that non-radial pulsation is responsible for part of the observed pattern (Figs. 9 and 10).

The sectorial ($\ell = 2, m = -2$) mode fails clearly to reproduce the observed variations, as the bumps take a full cycle

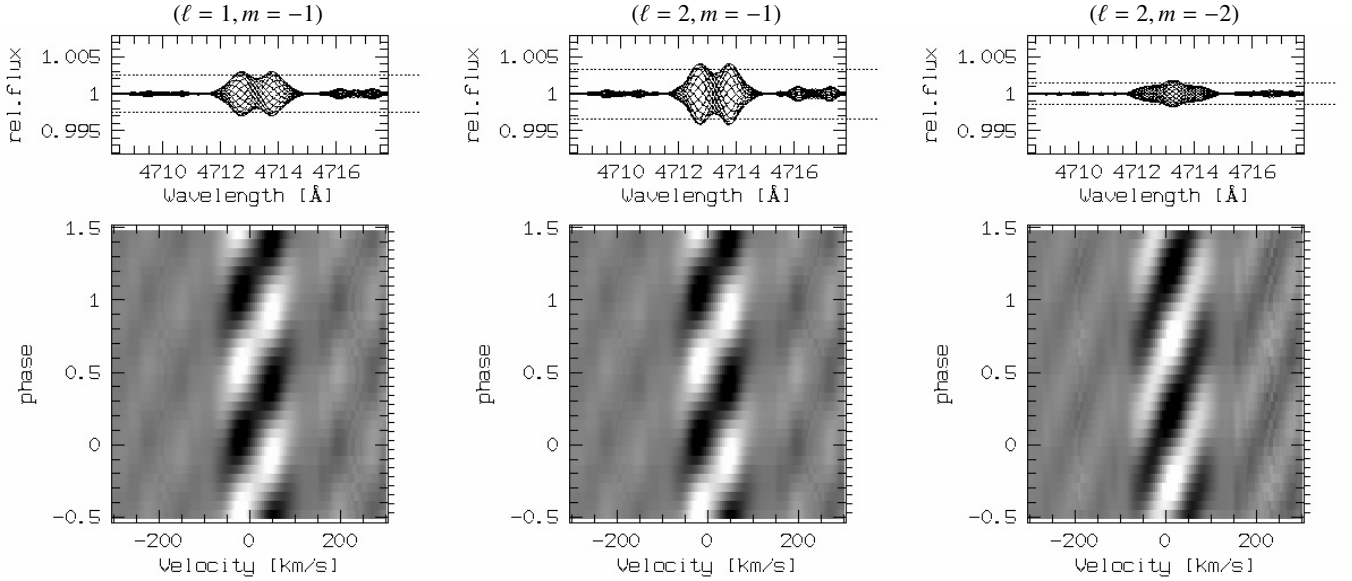

Fig. 10. Like Fig. 9, but for $v = 140\,\mathrm{km\,s^{-1}}$.

to cross the line profile from blue-to-red, not half a cycle as observed. The modes with $m = -1$ perform better when computed with low rotational velocities of 100 or 140 $\mathrm{km\,s^{-1}}$, i.e. close to the observed $v \sin i$, but become much worse when the rotation is increased and a more polar orientation is assumed. This might partly be a numerical problem, because the equatorial values for $\log g$ then are outside the implemented region, but the general result also holds for tests computed at higher values of $\log g$.

However, the $m = -1$ modes also do not reproduce all features of the observed variations. Importantly the S-type wave pattern is not reproduced. In Be stars analogous behaviour is explained with the help of a retrograde mode in a rapid rotator seen pole on (Rivinius et al. 2001; Maintz et al. 2003). However, the above considerations exclude retrograde modes, and test models computed with $m > 0$ confirm this. Only for the $m = -1$ modes in Fig. 10 is there a tentative indication of a central power minimum as part of a backward travelling feature, but this is still quite far from what is actually observed.

The $(\ell = 1, m = -1)$ and $(\ell = 2, m = -1)$ modes produce similar variations to each other. Any differences apparent in the distribution of variability power across the line profile (Fig. 9, upper row) are not significant at observational levels.

If ϵ Ori is a pulsating star, modes with $m = -1$ are the most likely ones, but they are not sufficient to explain the observed variations with this period entirely. For a full explanation further mechanisms would have to be assumed, such as interaction of the photospheric variations with the close circumstellar environment.

5. Final remarks

Some comparisons can be drawn between the differential radial velocity behaviour established here for ϵ Ori and the large velocity amplitude changes seen in the photospheric absorption lines of β Cepheid stars such as BW Vul (see e.g. Furenlid et al. 1987). Though the characteristic pulsational time-scale in the latter is usually several hours and not ∼days. In the case of BW Vul the optical photometric and radial velocity changes are also linked to variations in wind-formed UV resonance lines (see e.g. Massa 1994). These studies spotlight the role of deep-seated (photospheric) variations in inducing wind structure in high speed gas. Cranmer (1996) and Townsend (2000a,b) indicate that stellar pulsations arising deep in the interior can propagate toward the outer atmospheric layers as high-frequency gas pressure (p-mode) waves, or as lower frequency gravity (g-mode) waves. Their models which attempt to couple pulsation and an overlying wind suggest that the outflow can transport pulsational wave energy. This "wave-leakage" mechanism may permit stellar pulsations to initiate perturbations in the stellar wind regions. It remains to be worked out whether this process may be acting in ϵ Ori to provide a linear propagation of atmospheric wave signals into its stellar wind, resulting in the 1.9 day modulation.

Finally in advance of future studies of the dynamics of the wind-photosphere connection, we summarise the key optical line profile variability characteristics of ϵ Ori established in this paper:

1. The maximum central velocity amplitude of the line profile changes are $\pm 20\,\mathrm{km\,s^{-1}}$, but there is differential motion between spectral lines formed at different atmospheric depths (Figs. 2 and 3).
2. The fundamental time-scale of the main periodic component is ∼1.9 days. This principal cyclic behaviour has a "S-wave" pattern, which represents the blue-ward and red-ward swaying of the lines (Figs. 5 and 7).
3. There is a super-imposed second "S-wave" in the Balmer lines, which represents the most blue-ward progressing feature (Figs. 6 and 7). Its connection to the lower velocity "S-wave", which is seen largely within the limits of the projected rotation velocity, is not known The specific behaviour provides a fundamental discrepancy with

predictions from the standard non-radial pulsation models applied to ϵ Ori.

4. The ~1.9 day modulation is reasonably long-lived, since there is evidence for it in the HEROS data set from 1996 (Fig. 8). We cannot conclude about the long-term coherency of this cyclic behaviour from the present data.

Acknowledgements. We thank the staff at the European Southern Observatory (ESO) for their hospitality.

References

Baade 1998, in Cyclical Variability in Stellar Winds, ed. L. Kaper, & A. W. Fullerton (Springer), ESO Astrophys. Symp., 196
Blomme, R., Prinja, R. K., Runacres, M. C., & Colley, S. 2002, A&A, 921, 934
Cassinelli, J. P., Myers, R. V., Hartmann, L., Dupree, A. K., & Sanders, W. T. 1983, ApJ, 271, 681
Cranmer, S. 1996, Ph.D. Thesis, University of Delaware
Collura, A., Sciortino, S., Serio, S., et al. 1989, ApJ, 338, 296
De Jong, J. A., Henrichs, H. F., Kaper, L., et al. 2001, A&A, 368, 601
Ebbets, D. 1982, ApJS, 48, 399
Foing, B. H., Catala, C., Oliveira, J. M., et al. 1999, Adv. Space Res., 24, 251
Furenlid, I., Young, A., Meylan, T., Haag, C., & Crinklaw, G. 1987, ApJ, 319, 264
Fullerton, A. W., Gies, D. R., & Bolton, C. T. 1996, ApJS, 103, 475
Henrichs, H. F. 1998, in Variable and Non-spherical Stellar Winds in Luminous Hot Stars, ed. B. Wolf, O. Stahl, & A. W. Fullerton (Springer), IAU Coll. 169, LNP, 305
Jarad, M. M., Hilditch, R. W., & Skillen, I. 1989, MNRAS, 238, 1085
Kaufer, A., Prinja, R. K., & Stahl, O. 2002, A&A, 382, 1032
Kudritzki, R. P., Puls, J., Lennon, D. J., et al. 1999, A&A, 350, 970
Levato, H., Morrell, N., Garcia, B., & Malaroda, S. 1988, ApJS, 68, 319
Maintz, M., Rivinius, Th., Štefl, S., et al. 2003, A&A, 411, 181
Massa, D. 1994, Ap&SS, 221, 113
Massa, D., Fullerton, A. W., Nichols, J. S., et al. 1995, ApJ, 452, L53
Morrell, N., & Levato, H. 1991, ApJS, 75, 965
Prinja, R. K., Massa, D., & Fullerton, A. W. 2002, A&A, 388, 587
Reid, A. H. N., & Howarth, I. D. 1996, A&A, 311, 616
Rivinius, Th., Baade, D., Štefl, S., et al. 1998, A&A, 336, 177
Rivinius, Th., Baade, D., Štefl, S., et al. 2001, A&A, 369, 1058
Roberts, D. H., Lehár, J., & Dreher, J. W. 1987, AJ, 93, 968
Schaller, G., Schaerer, D., Meynet, G., & Maeder, A. 1992, A&AS, 96, 269
Scuderi, S. 1994, Ph.D. Thesis, University of Catania
Stahl, O., Kaufer, A., Wolf, B., et al. 1995, J. Astron. Data, 1, 3
Stahl, O., Kaufer, A., Rivinius, T., et al. 1996, A&A, 312, 539
Telting, J. H., & Schrijvers, C. 1997, A&A, 317, 723
Townsend, R. H. D. 1997, MNRAS, 284, 839
Townsend, R. H. D. 2000a, MNRAS, 318, 1
Townsend, R. H. D. 2000b, MNRAS, 319, 289
Walborn, N. R. 1976, ApJ, 205, 419